Spectrum of Externally Modulated Optical Signals

Keang-Po Ho, *Senior Member, IEEE,* and Joseph M. Kahn, *Fellow, IEEE*

***Abstract*—The optical power spectrum of a signal externally modulated using a Mach–Zehnder modulator is calculated analytically. Optical power spectra are calculated for binary signals for which the drive signal has either raised-cosine or Bessel-filtered pulse shape as well as for duobinary signals created by Bessel filtering. While the optical power spectrum is often approximated by the electrical power spectrum of the drive signal, this approximation usually underestimates the spectral spreading of the optical signal. Differences between the optical spectrum and the drive-signal electrical spectrum are most significant for drive signals having longer rise and fall times. Modulator chirp also broadens the optical spectrum. Chirp-induced spectral broadening is more significant for drive signals having longer rise and fall times.**

***Index Terms*—External modulator, optical networks, power spectrum.**

I. Introduction

MACH–ZEHNDER external modulators provide superior signal quality and are widely used in dense-wavelength-division-multiplexed (DWDM) systems. Compared with direct modulation or electroabsorption modulators, Mach–Zehnder external modulators yield smaller chirp, providing a narrower signal spectrum and usually resulting in a larger tolerance to uncompensated chromatic dispersion (considering both under- and overcompensation). Mach–Zehnder modulators (MZMs) can be made using various materials [1]–[6], and $LiNbO_3$ is the most popular material [1], [3]. Almost all commercial long-haul DWDM systems use $LiNbO_3$ MZMs.

Along with error probability and eye diagram, the optical spectrum of a signal is one of its most important attributes. In DWDM systems, the optical spectrum becomes especially important when the channel separation is small. When optical filters are used to separate adjacent wavelength-division-multiplexed (WDM) channels, interchannel crosstalk depends on the optical spectrum. Literature on WDM systems commonly shows the measured or simulated optical spectra of optical signals. However, to our knowledge, no analytical method has been presented to calculate the spectrum of an externally modulated optical signal. An MZM separates an optical signal into two paths, which are phase-modulated and then combined. Because the modulator is based on two correlated phase modulators, analysis of the optical spectrum is difficult.

The optical spectrum has often been approximated using the electrical spectrum of the drive signal, especially when a zero-chirp modulator is employed. As shown subsequently, this approximation is valid only for wide-band drive signals that are close to a rectangular pulse shape. In the practical cases of a band-limited drive signal or a chirped modulator, this approximation always underestimates the spectral spread of the optical signal. If the drive signal has long rise and fall times, this approximation significantly underestimates the spectral spread, even when a zero-chirp modulator is used.

The remainder of this paper is organized as follows. Section II derives the optical spectrum of a binary signal with a chirped modulator. Section III derives the optical spectrum of a binary signal with either raised-cosine or Bessel-filtered pulse shape. Section IV derives the optical spectrum of a duobinary signal created by Bessel filtering. Finally, Section V presents the conclusions of the paper.

II. Derivation of Optical Spectrum of Binary Signal

An MZM has many different possible configurations [1]. The most general case is a dual-drive modulator with two possibly independent drive signals. A single-drive modulator can be modeled using a dual-drive modulator in which the two driving voltages have a fixed relationship.

When an MZM is biased at the middle inflection point and the drive signal has a peak-to-peak voltage of V_π, the normalized baseband representation of the electric field at the output of the modulator is

$$e(t) = \frac{1}{2}\left\{\exp\left[\frac{j(1+\alpha)\pi}{4}\phi(t)\right] + j\exp\left[-\frac{j(1-\alpha)\pi}{4}\phi(t)\right]\right\} \tag{1}$$

where α is the chirp coefficient [7], and $\phi(t)$ is the normalized binary drive signal

$$\phi(t) = \sum_{k=-\infty}^{+\infty} b_k p(t - kT) \tag{2}$$

where $b_k = \pm 1$ is the transmitted random data stream, $p(t)$ is the pulse shape of the drive signal, and T is the bit interval of the data. The two terms in (1) correspond to the two phase-modulated paths of the MZM. The differential phase shift between the two phase modulators is $\pi\phi(t)/2$. The normalized intensity of the modulator output $|e(t)|^2 = \sin[\pi(1+\phi(t))/4]^2$ is independent of the chirp coefficient. The relation (1) can be used to model all types of MZMs having different values of chirp coefficient α. For example, a dual-drive modulator has adjustable

Manuscript received March 19, 2003. This work was supported at National Taiwan University in part by the National Science Council under Grant NSC-92-2218-E-002-034 and at Stanford University in part by the National Science Foundation under Grant ECS-0335013.

K.-P. Ho is with the Institute of Communication Engineering and Department of Electrical Engineering, National Taiwan University, Taipei 106, Taiwan, R.O.C. (e-mail: kpho@cc.ee.ntu.edu.tw).

J. M. Kahn is with the Department of Electrical Engineering, Stanford University, Stanford, CA 94305 USA, and also with StrataLight Communications, Campbell CA 95008 USA (e-mail: jmk@ee.stanford.edu).

Digital Object Identifier 10.1109/JLT.2004.824453

chirp [8], a single-drive z-cut modulator has a chirp coefficient $\alpha = \pm 0.75$ [9], and an x-cut push–pull MZM has zero chirp. Because most external modulators have very large extinction ratios, the expression (1) assumes an infinite extinction ratio. A finite extinction ratio may contribute a small amount of chirp into the optical signal [10], [11].

The random process (1) is cyclo-stationary with a period of T and has an average autocorrelation function of

$$\overline{R}(\tau) = \frac{1}{T}\int_0^T R(t+\tau, t)dt \tag{3}$$

where the autocorrelation function is $R(t+\tau, t) = E\{e(t+\tau)e^*(t)\}$, where $E\{\cdot\}$ denotes expectation. Because $\overline{R}(\tau) = \overline{R}^*(-\tau)$, the power spectral density is

$$\Phi_e(f) = 2\Re\left\{\int_0^{+\infty} \overline{R}(\tau)\exp(-j2\pi f\tau)d\tau\right\} \tag{4}$$

where $\Re\{\cdot\}$ denotes the real part of a complex number.

The autocorrelation function $R(t+\tau, t)$ is

$$\begin{aligned} R(t+\tau,t) =& \frac{1}{4}E\left\{\exp\left[\frac{j(1+\alpha)\pi}{4}(\phi(t+\tau)-\phi(t))\right]\right\} \\ &+ \frac{1}{4}E\left\{\exp\left[\frac{j(1-\alpha)\pi}{4}(\phi(t+\tau)-\phi(t))\right]\right\} \\ &- \frac{j}{4}E\Big\{\exp\Big[\frac{j(1+\alpha)\pi}{4}\phi(t+\tau) \\ &\qquad + \frac{j(1-\alpha)\pi}{4}\phi(t)\Big]\Big\} \\ &+ \frac{j}{4}E\Big\{\exp\Big[-\frac{j(1+\alpha)\pi}{4}\phi(t+\tau) \\ &\qquad - \frac{j(1-\alpha)\pi}{4}\phi(t)\Big]\Big\}. \end{aligned} \tag{5}$$

The terms in (5) need to be calculated one by one. First, using (2) and assuming that binary bits $b_k = \pm 1$ have equal probability, similar to the approach of [12] and [13], the first term of (5) is

$$\begin{aligned} &E\left\{\exp\left[\frac{j(1+\alpha)\pi}{4}(\phi(t+\tau)-\phi(t))\right]\right\} \\ &= \prod_{k=-\infty}^{+\infty}\cos\left\{\frac{(1+\alpha)\pi}{4}[p(t+\tau-kT)-p(t-kT)]\right\}. \end{aligned} \tag{6}$$

The second term of (5) is

$$\begin{aligned} &E\left\{\exp\left[\frac{j(1-\alpha)\pi}{4}(\phi(t+\tau)-\phi(t))\right]\right\} \\ &= \prod_{k=-\infty}^{+\infty}\cos\left\{\frac{(1-\alpha)\pi}{4}[p(t+\tau-kT)-p(t-kT)]\right\}. \end{aligned} \tag{7}$$

The third and fourth terms in (5) sum to zero. The fourth term is the complex conjugate of the third term. The summation of the third and fourth terms is also the complex conjugate of itself and must be a real number. Because both the third and fourth terms are purely imaginary numbers, the summation of the third and fourth terms is equal to zero.

Using (3) and (5)–(7), the average autocorrelation function is

$$\overline{R}(\tau) = \frac{1}{4}\overline{R}_\gamma\left(\tau, \frac{(1+\alpha)\pi}{4}\right) + \frac{1}{4}\overline{R}_\gamma\left(\tau, \frac{(1-\alpha)\pi}{4}\right) \tag{8}$$

where

$$\overline{R}_\gamma(\tau,\gamma) = \frac{1}{T}\int_0^T \prod_{k=-\infty}^{+\infty}\cos\{\gamma[p(t+\tau-kT)-p(t-kT)]\}dt \tag{9}$$

where γ can be considered as the modulation index of the signal. From the average autocorrelation function (8), we see that both the average autocorrelation function and the power spectral density are independent of the sign of the chirp coefficient. Chirp coefficients of $\pm\alpha$ give identical power spectral densities. Because the average autocorrelation function $\overline{R}(\tau)$ is a real even function, the power spectral density $\Phi_e(f)$ is a real even function. In subsequent sections of this paper, we only plot the positive-frequency side of $\Phi_e(f)$.

Similar to the approach of [12], the average autocorrelation function (9) can be calculated for different values of the modulation index γ. The pulse $p(t)$ is centered around $t = 0$. Assume that $|p(t)| \geq \epsilon$ if and only if $-KT \leq t \leq MT$, where ϵ is a small positive number, and K and M are two integers. For $|\tau| \geq (M+K)T$, the pulses $p(t-kT)$ and $p(t+\tau-kT)$ do not overlap with each other for all values of k. Letting $\tau = \xi + nT$, where the variable ξ is confined to $0 \leq \xi \leq T$ and n is an integer larger than $M+K$, we get

$$\begin{aligned} \overline{R}(\xi+nT,\gamma) =& \frac{1}{T}\int_0^T \prod_{m=-(M-1)}^{K}\cos[\gamma p(t-mT)] \\ &\times \prod_{m=-(M-1)}^{K+1}\cos[\gamma p(t+\xi-mT)]dt \end{aligned} \tag{10}$$

where $n \geq M+K$. For $|\tau| \geq (M+K)T$, the average autocorrelation function $\overline{R}(\tau,\gamma)$ is a periodic function having period T.

For $|\tau| < (M+K)T$, the average autocorrelation function is

$$\begin{aligned} \overline{R}(\tau,\gamma) = \frac{1}{T}\int_0^T \prod_{m=-(M-1)}^{K+\lceil\tau/T\rceil}\cos\{\gamma[p(t+\tau-mT) \\ -p(t-mT)]\}dt \end{aligned} \tag{11}$$

where the symbol $\lceil x\rceil$ denotes the smallest integer greater than or equal to x. Using both (10) and (11), the average autocorrelation function (8) can be calculated by the summing the two cases with $\gamma = (1\pm\alpha)\pi/4$. The average autocorrelation function $\overline{R}(\tau)$ also has two parts, corresponding to (10) and (11), respectively. For $|\tau| \geq (M+K)T$, the average autocorrelation function $\overline{R}(\tau)$ is also a periodic function having period T.

Taking into account the two parts of the average autocorrelation function $\overline{R}(\tau)$, using (4), we get

$$\begin{aligned} \Phi_e(f) =& 2\Re\left\{\int_0^{(K+M)T}\left[\overline{R}(\tau)\right.\right. \\ &\left.\left. -\overline{R}(\tau+KT+MT)\right]e^{-i2\pi f\tau}d\tau\right\} \\ &+ \frac{1}{T}\sum_{n=-\infty}^{+\infty}\delta\left(f-\frac{n}{T}\right) \\ &\times \int_0^T \Re\left\{\overline{R}(\xi+KT+MT)e^{-i2\pi n\xi/T}\right\}d\xi \end{aligned} \tag{12}$$

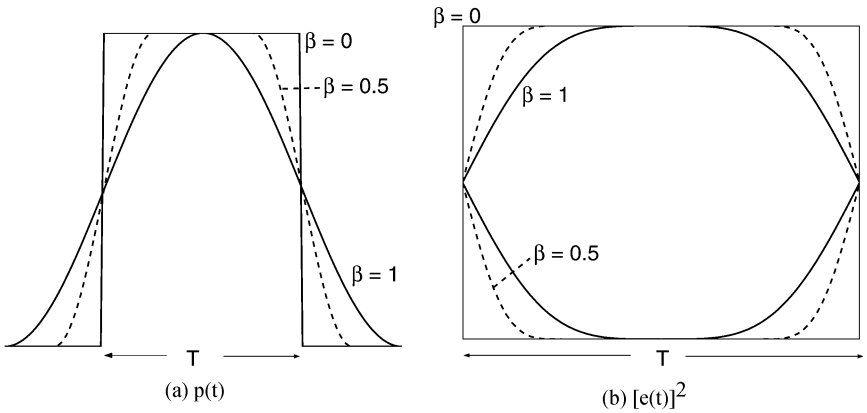

Fig. 1. (a) Raised-cosine pulse shape and (b) the corresponding eye opening.

where the first term is the continuous spectrum corresponding to (11) for $|\tau| \leq (K+M)T$, and the second term consists of discrete tones at frequencies n/T, $n = 0, \pm 1, \pm 2, \ldots$, corresponding to the periodic autocorrelation function (10) for $|\tau| > (K+M)T$.

The optical spectrum of the signal (1) is often approximated by the electrical spectrum of the drive signal (2). The drive signal (2) has an electrical power spectral density of

$$\Phi_\phi(f) = \frac{1}{T}|P(f)|^2 \tag{13}$$

where $P(f)$ is the Fourier transform of the pulse $p(t)$. Comparing the spectra (12) and (13), an obvious difference is the appearance of discrete tones in the optical spectrum $\Phi_e(f)$ given by (12). In particular, the tone at $f = 0$ is due to the average electric field, which carries no information.

III. Numerical Results of Optical Spectrum of Binary Signal

Using the analytical formulas given in Section II, the power spectral density of random data stream having either raised-cosine or Bessel-filtered pulse are evaluated in this section.

A. Raised-Cosine Pulse

The raised-cosine pulse is

$$p(t) = \begin{cases} 1, & |t| < (1-\beta)\frac{T}{2} \\ \frac{1}{2}\left[1 - \sin\left(\frac{\pi\left(|t| - \frac{T}{2}\right)}{\beta T}\right)\right], & |t| \geq (1-\beta)\frac{T}{2} \\ & |t| \leq (1+\beta)\frac{T}{2} \\ 0, & |t| > (1+\beta)\frac{T}{2} \end{cases} \tag{14}$$

where $0 \leq \beta \leq 1$ is the roll-off factor. The rectangular pulse corresponds to a zero roll-off factor $\beta = 0$. Fig. 1 plots the raised-cosine pulse shape and the corresponding optical eye opening. The definition of raised-cosine pulse in (14) is not the same as that in standard digital communication textbooks, e.g., [14]. In (14), the pulse is defined to be a raised cosine in the time domain, in order to time-limit the pulse. The pulse (14) has smooth rising and falling edges with well-defined rise and fall times of $0.59\beta T$. The raised-cosine pulse is equal to zero for $t \geq T$, limiting the spectral density (12) to terms for $K = M = 1$, simplifying the calculation procedure. Comparing the pulse shape Fig. 1(a) and the eye opening Fig. 1(b), we see that the MZM's nonlinear transfer characteristic modifies the waveform substantially. Because the rise and fall times of the optical intensity are shortened to $0.40\beta T$, the optical spectrum broadens accordingly. However, an analysis based solely on the eye diagram of Fig. 1(b) cannot take into account the effects of modulator chirp upon the optical spectrum.

Fig. 2 show the single-sided power spectral density of the optical signal (12) modulated by a random pulse stream with the raised-cosine pulse shape of Fig. 1(a). Values of the roll-off factor $\beta = 0.5$ and $\beta = 1$ are shown in Fig. 2(a) and (b), respectively. Fig. 2 also shows the power spectral densities for different values of the chirp coefficient $\alpha = 0, \pm 0.5, \pm 1$. The case of a rectangular pulse $\beta = 0$ is shown in both Fig. 2(a) and (b) for comparison. Fig. 2 also plots the electrical spectrum of the drive signal $\Phi_\phi(f)$ calculated by (13) for comparison.

When the drive signal is a rectangular pulse with $\beta = 0$, the power spectral density is independent of the chirp coefficient, and the optical power spectral density (12) is identical to the electrical power spectral density of the drive signal given by (13).

When the drive signal is a low-pass-filtered signal with nonzero roll-off factor $\beta > 0$, a nonzero chirp coefficient broadens the optical spectrum. Fig. 2 shows that approximating the optical spectrum by the electrical spectrum of the drive signal (13) underestimates the spectral spread of the optical signal. In Fig. 2, we see major differences at the normalized frequencies $fT = \pm 1, \pm 2, \ldots$. While the electrical spectrum of the drive signal (13) has notches at those normalized frequencies, the optical spectrum (12) has discrete tones at those same frequencies and also has a tone at $f = 0$ due to the dc value of the electric field (1). In Fig. 2(b), for $\beta = 1$, the electrical spectrum (13) has notches at the normalized frequencies $fT = \pm 1.5, \pm 2.5, \ldots$, while the optical spectrum (12) has nonzero values at those frequencies.

The differences between the power spectra (12) and (13) are more significant when the raised-cosine pulse (14) has a larger roll-off factor, corresponding to longer rise and fall times. When the roll-off factor is $\beta = 0.5$ in Fig. 2(a), at the second lobe of the spectrum at $fT \approx 1.5$, the difference is about 3 dB and increases with increasing chirp coefficient. When the roll-off

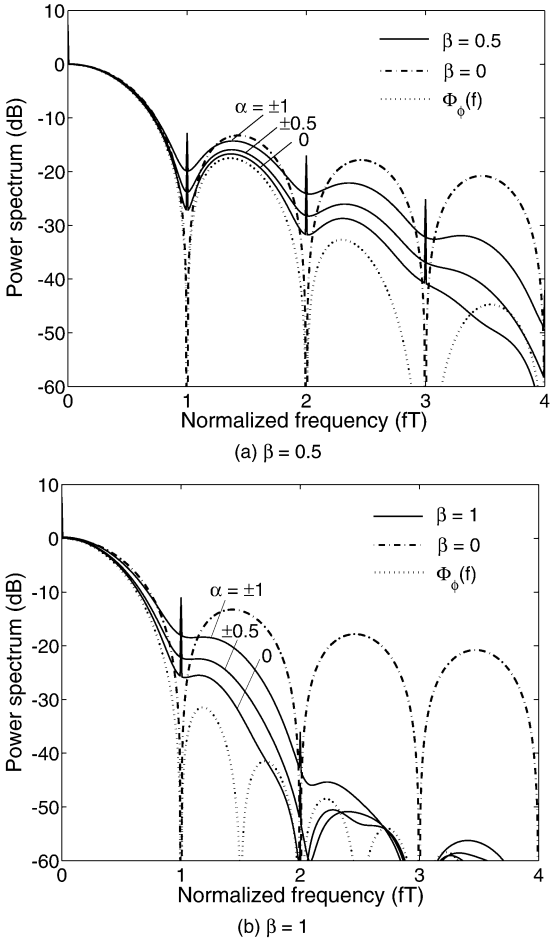

Fig. 2. Power spectral density of the optical signal when raised-cosine pulse with roll-off factors of (a) $\beta = 0.5$ and (b) $\beta = 1$ are used.

factor is $\beta = 1$ in Fig. 2(b), at the second lobe of the spectrum at $fT \approx 1.25$, the difference is about 5–12 dB and increases with an increasing chirp coefficient.

The effect of the chirp coefficient depends on the pulse roll-off factor β. As discussed previously, for a rectangular pulse $\beta = 0$, the chirp coefficient does not affect the optical power spectral density (12). With a roll-off factor of $\beta = 0.5$, the chirp coefficient does not change the optical power spectral density (12) as much as when the roll-off factor takes on the larger value $\beta = 1$. By comparing Fig. 2(a) with Fig. 2(b), we may conclude that the chirp coefficient has a greater effect on the optical spectrum for a drive signal (2) having longer rise or fall times.

B. Bessel-Filtered Pulse

In idealized simulations, excellent results are obtained driving an MZM by an ideal rectangular pulse that has been filtered by a Bessel low-pass filter. Fig. 3 shows both the pulse shape and the corresponding eye opening when a fifth-order Bessel filter having a bandwidth of either $0.75/T$ or $0.5/T$ is used. Owing to the nonlinear transfer characteristic of the MZM, a bandwidth of $0.5/T$ is sufficient to provide an open eye, but then the receiver must have a very wide bandwidth to preserve the eye opening at the decision circuit.

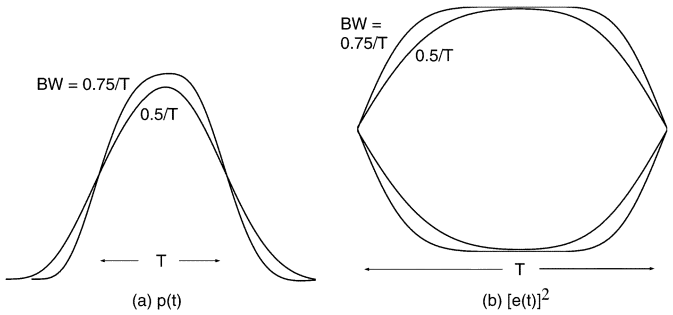

Fig. 3. (a) Bessel-filtered pulse shape and (b) the corresponding eye opening.

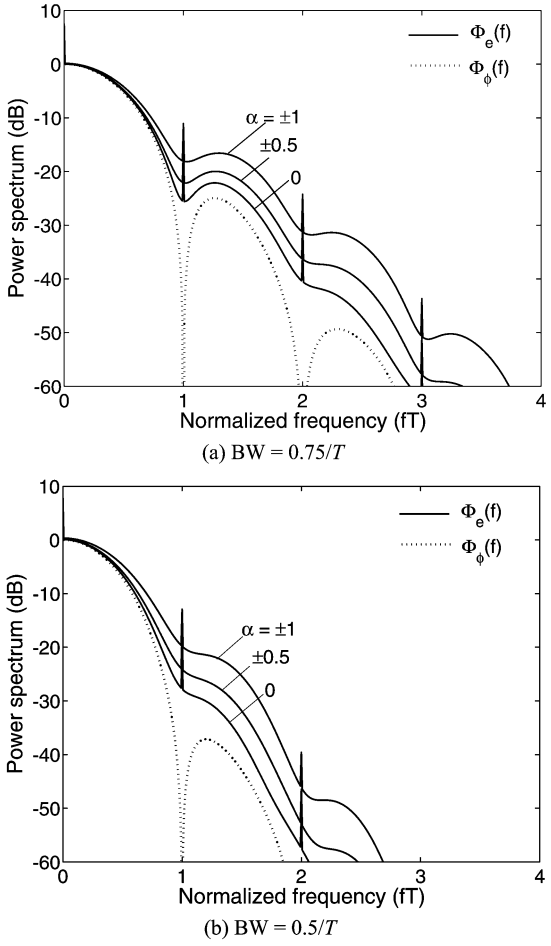

Fig. 4. Power spectral density of the optical signal when a Bessel-filtered pulse is used. The Bessel filter has a bandwidth of (a) $0.75/T$ and (b) $0.5/T$.

Fig. 4 shows the single-sided optical spectrum of the optical signal modulated by a random pulse stream with a Bessel-filtered pulse given by Fig. 3(a). Fifth-order Bessel filters having bandwidths of $0.75/T$ and $0.5/T$ are used in Fig. 4(a) and (b), respectively. Fig. 4 also shows the optical spectrum for different values of the chirp coefficient $\alpha = 0, \pm 0.5, \pm 1$. For comparison, Fig. 4 also plots the electrical spectrum of the drive signal $\Phi_\phi(f)$, calculated using (13).

Modulator chirp broadens the optical spectrum of the signal (12). Similar to Fig. 2, Fig. 4 shows that approximating the optical spectrum using the electrical spectrum of the drive signal (13) underestimates the spectral spreading. The differences between the power spectra of (12) and (13) are more significant

when the low-pass filter having the smaller bandwidth of $0.5/T$ is used. Similar to Fig. 2, Fig. 4 shows that chirp broadens the optical spectrum, causing more broadening when a Bessel filter having smaller bandwidth, corresponding to longer rise and fall times, is used.

IV. Spectrum of Optical Duobinary Signal

Optical duobinary signals can be generated by many different methods, and the use of a Bessel-filtered pulse with a filter bandwidth of about $0.28/T$ is one of the simplest and most popular implementations [15]–[17]. The low-pass filter converts the binary electrical signal to a three-level drive signal. Modulation is performed using a zero-chirp MZM biased at the minimum transmission point. The drive signal has a peak-to-peak voltage of $2V_\pi$. A binary receiver can be used because the modulator converts the three-level electrical drive signal to an optical signal having three field levels, but only two intensity levels. The normalized baseband representation of the electric field at the modulator output is

$$e(t) = \frac{1}{2}\left\{\exp\left[\frac{j\pi}{2}\phi(t)\right] - \exp\left[-\frac{j\pi}{2}\phi(t)\right]\right\} \tag{15}$$

where $\phi(t)$ is defined as in (2) and where b_k represents the precoded data. The electric field (15) is a three-level duobinary signal, but the optical intensity $|e(t)|^2$ is similar to a conventional binary signal [15]. The optical power spectrum (15) has been measured routinely [16], [17] but has never been analytically calculated. Following the procedure from (5) –(9), the average autocorrelation function of (15) is

$$\begin{aligned}\overline{R}(\tau) = &\frac{1}{2T} \\ &\times \int_0^T \prod_{k=-\infty}^{+\infty} \cos\Big\{\frac{\pi}{2}\Big[p(t+\tau-kT) \\ &\qquad - p(t-kT)\Big]\Big\}dt \\ &- \frac{1}{2T} \\ &\times \int_0^T \prod_{k=-\infty}^{+\infty} \cos\Big\{\frac{\pi}{2}\Big[p(t+\tau-kT) \\ &\qquad + p(t-kT)\Big]\Big\}dt. \end{aligned} \tag{16}$$

Following the procedure from (10) to (12), the power spectral density of the optical signal of (15) can be found using the average autocorrelation function of (16).

Fig. 5 shows the single-sided optical spectrum of a duobinary signal, obtained by calculating $\Phi_e(f)$ given by (12) using the average autocorrelation function (16). The electrical power spectral density of the drive signal is also shown for comparison. Because the average autocorrelation function approaches zero, i.e., $\overline{R}(\tau) = 0$ for large timing differences $|\tau| > (K+M)T$, there are no discrete tones in the optical spectrum (12). Fig. 5 shows a 20–dB difference between the optical power spectrum $\Phi_e(f)$ and the electrical spectrum of the drive signal $\Phi_\phi(f)$ at normalized frequencies near $fT = 1.25$. Even when a zero-chirp modulator is used, the optical power spectrum given by (12) is far broader than the electrical spectrum of the drive signal (13), because of the small filter bandwidth of $0.28/T$.

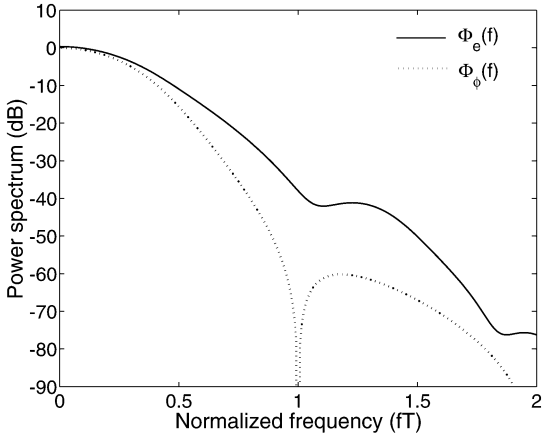

Fig. 5. Optical power spectral density of duobinary signals.

V. Conclusion

The power spectral density of an external modulated optical signal has been derived analytically for the first time. Optical spectra are calculated for binary signals with both raised-cosine and Bessel-filtered drive signal pulse shapes, and for optical duobinary signals created by Bessel filtering. Approximating the optical spectrum using the electrical spectrum of the drive signal significantly underestimates the spectral spreading. The differences are more significant when the drive signal has longer rise and fall times. Modulator chirp broadens the optical power spectrum, and the broadening is more significant when the drive signal has longer rise and fall times.

References

[1] E. L. Wooten, K. M. Kissa, A. Yi-Yan, E. J. Murphy, D. A. Lafaw, P. F. Hallemeier, D. Maack, D. V. Attanasio, D. J. Fritz, G. J. McBrien, and D. E. Bossi, "A review of Lithium Niobate modulators for fiber-optic communications systems," *IEEE J. Select. Topics Quantum Electron.*, vol. 6, pp. 69–82, Jan.–Feb. 2000.

[2] M. Erman, P. Jarry, R. Gamonal, P. Autier, J.-P. Chane, and P. Frijlink, "Mach–Zehnder modulators and optical switches on III–V semiconductors," *J. Lightwave Technol.*, vol. 6, pp. 837–846, June 1988.

[3] R. C. Alferness, "Titanium-diffused Lithium Noibate waveguide devices," in *Guided-Wave Optoelectronics*, T. Tamir, Ed. Berlin, Germany: Springer-Verlag, 1990, pp. 145–210.

[4] F. J. Leonberger and J. P. Donnelly, "Semiconductor integrated optic devices," in *Guided-Wave Optoelectronics*, T. Tamir, Ed. Berlin, Germany: Springer-Verlag, 1990, pp. 317–396.

[5] J. Yu, C. Rolland, A. Somani, S. Bradshaw, and D. Yevick, "Phase-engineered III–V MQW Mach-Zehnder modulator," *IEEE Photon. Technol. Lett.*, vol. 8, pp. 1018–1020, Aug. 1996.

[6] Y. Shi, C. Zhang, H. Zhang, J. H. Bechtel, L. R. Dalton, B. H. Robinson, and W. H. Steier, "Low (sub-1-volt) halfwave voltage polymeric electro-optic modulators achieved by controlling chromophore shape," *Science*, vol. 288, pp. 119–122, Apr. 2000.

[7] F. Koyama and K. Oga, "Frequency chirping in external modulators," *J. Lightwave Technol.*, vol. 6, pp. 87–93, Jan. 1988.

[8] A. H. Gnauck, S. K. Korotky, J. J. Veselka, J. Nagel, C. T. Kemmerer, W. J. Minford, and D. T. Moser, "Dispersion penalty reduction using an optical modulator with adjustable chirp," *IEEE Photon. Technol. Lett.*, vol. 3, pp. 916–918, Oct. 1991.

[9] M. Schiess and H. Carlden, "Evaluation of the chirp parameter of a Mach–Zehnder intensity modulator," *Electron. Lett.*, vol. 30, pp. 1524–1525, 1994.

[10] H. Kim and A. H. Gnauck, "Chirp characteristics of dual-drive, Mach–Zehnder modulator with a finite DC extinction ratio," *IEEE Photon. Technol. Lett.*, vol. 12, pp. 298–300, Mar. 2002.

[11] S. Walklin and J. Conradi, "Effect of Mach–Zehnder modulator DC extinction ratio on residual chirp-induced dispersion in 10-Gb/s binary and AM-PSK duobinary lightwave systems," *IEEE Photon. Technol. Lett.*, vol. 9, pp. 1400–1402, Oct. 1997.
[12] K.-P. Ho, "Spectral density of cross-phase modulation induced phase noise," *Opt. Commun.*, vol. 169, pp. 63–68, 1999.
[13] K.-P. Ho, E. Kong, L. Y. Chan, L.-K. Chen, and F. Tong, "Analysis and measurement of root-mean-squared bandwidth of cross-phase modulation induced spectral broadening," *IEEE Photon. Technol. Lett.*, vol. 11, pp. 1126–1128, Sept. 1999.
[14] J. G. Proakis, *Digital Communications*, 4 ed. Boston, MA: McGraw-Hill, 2000, pp. 559–561.
[15] A. J. Price and N. L. Mercier, "Reduced bandwidth optical digital intensity modulation with improved chromatic dispersion tolerance," *Electron. Lett.*, vol. 31, pp. 58–59, 1995.
[16] T. Ono, Y. Yano, K. Fukuchi, T. Ito, H. Yamazaki, M. Yamaguchi, and K. Emura, "Characteristics of optical duobinary signals in terabits/s capacity, high-spectral efficiency WDM systems," *J. Lightwave Technol.*, vol. 16, pp. 788–797, May 1998.
[17] H. Kim and C. X. Yu, "Optical duobinary transmission system featuring improved receiver sensitivity and reduced optical bandwidth," *IEEE Photon. Technol. Lett.*, vol. 14, pp. 1205–1207, Aug. 2002.

Keang-Po Ho (S'91–M'95–SM'03) received the B.S. degree from National Taiwan University, Taipei, Taiwan, in 1991 and the M.S. and Ph.D. degrees from the University of California at Berkeley in 1993 and 1995, respectively, all in electrical engineering.

He performed research on all-optical networks with IBM T. J. Watson Research Center, Hawthorne, NY, in summer 1994. He was a Research Scientist with Bellcore, currently Telcordia Technologies, Red Bank, NJ, from 1995 to 1997, conducting research on optical networking, high-speed lightwave systems, and broad-band access. He taught in the Department of Information Engineering of the Chinese University of Hong Kong from 1997 to 2001. He served as the Chief Technology Officer of StrataLight Communications, Campbell, CA, from 2000 to 2003, developing spectral efficiency 40-Gb/s lightwave transmission systems. He has been with the Institute of Communication Engineering and Department of Electrical Engineering, National Taiwan University, since 2003. His research interests include optical communication systems, multimedia communication systems, combined source-channel coding, and communication theory. He was among the pioneers for research on hybrid wavelength-division-multiplexing (WDM) systems, combined source-channel coding using multi-carrier modulation or Turbo codes, and performance evaluation of phase-shift keying (PSK) and differential PSK (DPSK) signals with nonlinear phase noise. He has published more than 130 journal and conference articles in those fields.

Joseph M. Kahn (F'00) received the A.B., M.A., and Ph.D. degrees in physics from the University of California at Berkeley (U.C. Berkeley) in 1981, 1983, and 1986, respectively.

From 1987 to 1990, he was with the Crawford Hill Laboratory, AT&T Bell Laboratories, Holmdel, NJ. He demonstrated multi-gigabit-per-second coherent optical fiber transmission systems, setting world records for receiver sensitivity. From 1990 to 2003, he was a Member of the faculty of the Department of Electrical Engineering and Computer Sciences at U.C. Berkeley, performing research on optical and wireless communications. Currently, he is an Adjunct Professor in that department. Since 2003, he has also been a Professor of Electrical Engineering at Stanford University, Stanford, CA. He is also currently a Professor at StrataLight Communications, Campbell, CA. His current research interests include single- and multi-mode optical fiber communications, free-space optical communications, and microelectromechanical systems (MEMS) for optical communications.

Prof. Kahn received the National Science Foundation Presidential Young Investigator Award in 1991. From 1993 to 2000, he served as a Technical Editor of the *IEEE Personal Communications Magazine*.